Synthesis and Characterization of the Microporosity of Ion-Exchanged Al_2O_3-Pillared Clays

Nick D. Hutson, Donald J. Gualdoni, and Ralph T. Yang*

Department of Chemical Engineering University of Michigan Ann Arbor, Michigan 48109

Received June 26, 1998. Revised Manuscript Received September 17, 1998

We have studied the effects of postsynthesis ion exchange on the microporous properties of Al_2O_3-pillared clays. These changes were effected by incorporating differently-sized charge-compensating cations from the alkali and alkaline earth series into the pillared clay by standard ion-exchange techniques. The resulting materials were characterized with respect to their surface area, interlayer spacing, and micropore size distribution. The micropore size distributions were determined from their N_2 adsorption isotherms at 77 K using the slit-pore model of the Horvath−Kawazoe equation (and applying the Cheng−Yang correction). The results showed a bimodal micropore size distribution for the unaltered pillared clay and for all of the ion-exchanged pillared clays. In every case, the micropore volume for those pores in the lower distribution (<0.45 nm) increased with increasing ionic radius of the charge-compensating cations used in the ion exchange. In each case, the micropore volume for those pores in the upper distribution (>0.45 nm) decreased with ion exchange. X-ray diffraction (XRD) analysis showed the ion-exchange procedure had no effect on the interlayer spacings of the pillared clays. In all cases, the peak pore sizes were less than the free interlayer spacing as determined by XRD analysis. Dubinin−Astakhov-transformed isotherms were used to qualitatively characterize the micropore distribution of the clays. The Dubinin−Astakhov equation was used to determine the effect of postsynthesis ion exchange on the relative structural and energetic heterogeneity of the material.

Introduction

Pillared interlayered clays (PILCs), or pillared clays, are a class of porous, high surface area, two-dimensional materials that have been studied extensively for application as catalysts and, to a lesser degree, as sorbents for gas separations. These materials are prepared by exchanging the charge-compensating cations between the clay layers with larger inorganic hydroxy cations, which are polymeric or oligomeric hydroxy metal cations formed by hydrolysis of metal salts.[1] Upon calcination, these metal hydroxy cations undergo dehydration and dehyroxylation. The result is a material with stable metal oxide clusters acting as pillars to separate the clay layers and creating interlayer and interpillar spacings of molecular dimension. Comprehensive reviews of the subject are available.[2−4]

Although most PILC studies have focused on their use for catalytic application, there has also been other work in which PILCs have been studied as potential sorbents for gas separation applications. Kinetic separations are those in which the separation is effected by differences in diffusion rates into the sorbent. An example of a commercial application that employs kinetic separation is that of air using carbon molecular sieves (CMSs). In this case, the nitrogen and oxygen are separated because O_2 diffuses faster than N_2 in the CMSs. Other promising kinetic separations have included the CO_2/CH_4 separation,[5] and the N_2/CH_4 separation,[6] both using CMSs, and separation of air using 4A zeolite.[7,8] For type-A zeolites, the pore size is controlled sterically by the use of differently-sized charge-compensating cations. The Na^+ ion is used as the charge-compensating cation for 4A zeolite, whereas K^+ and Ca^{2+} are used for 3A and 5A zeolites, respectively. Successful kinetic separations are dependent on the effectiveness of the sorbent; and the effective sorbent will tend to have a reliable distribution of micropores centered around a very small average pore diameter (approximately 0.5 nm). Ion-exchanged PILCs have been considered for air separation.[9,10] The cation exchange capacity of PILCs can be altered by various treatments.[10,11]

When designing materials for application in kinetic separations, evaluation of the porosity is a necessary step in the overall characterization of the material of interest. The meso- and macroporosity can be characterized using the Kelvin equation (e.g., the Barrett−Joyner−Halenda (BJH) model); however, the Kelvin equation is restricted to pore sizes >2 nm and is, hence,

* To whom correspondence should be addressed.

(1) Cheng, L. S.; Yang, R. T. *Microporous Mater.* **1997**, *8*, 177.
(2) Pinnavaia, T. J. *Science* **1983**, *220*, 365.
(3) Burch, R. *Pillared Clays In Catalysis Today*, Vol. 2; Elsevier: New York, 1988; p 185.
(4) Figueras, F. *Catal. Rev. Sci. Eng.* **1988**, *30*, 457.
(5) Kapoor, A.; Yang, R. T. *Chem. Eng. Sci.* **1989**, *44*, 1723.
(6) Ackley, M. W.; Yang, R. T. *AIChE J.* **1990**, *36*, 1229.
(7) Shin, H. S.; Knaebel, K. S. *AIChE J.* **1987**, *33*, 654.
(8) Pan, Z.; Yang, R. T.; Ritter, J. A. *Kinetic separation of air by PSA. New Directions in Sorption Technology;* Keller, G. E., Jr.; Yang, R. T., Eds.; Butterworth: Boston, 1989.
(9) Molinard, A.; Vansant, E. F., in *Separation Technology*; Vansant, E. F., Ed.; Elsevier: Amsterdam, 1994; p 423.
(10) Cheng, L. S.; Yang, R. T. *Ind. Eng. Chem. Res.* **1995**, *34*, 2021.
(11) Li, D. Y.; Scala, A. A.; Ma, Y. H., *Adsorption*, **1996**, *2*, 227.

10.1021/cm980454j CCC: $15.00
Published on Web 10/31/1998

not applicable for characterization of the microporosity. Simple models have been proposed for calculating the micropore size distribution and the potential energy profiles for molecular sieves. Everett and Powl[12] have calculated the potential energy profiles for adsorption on slit-shaped pores. Horvath and Kawazoe[13] used the slit-shape model to develop a simple method for calculation of the effective micropore size distribution using the adsorption isotherm data for molecular sieve carbon. This Hovarth and Kawazoe (H−K) equation has been further enhanced to accommodate spherical[14] and cylindrical[15] pore geometries.

Gil and Montes[16] studied the microporosity of Al_2O_3-pillared clays prepared with different Al/clay ratios. The authors used nitrogen adsorption isotherm data taken at very low relative pressures to characterize the microporosity of the intercalated materials. Gil et al.[17] similarly used the nitrogen isotherm data to characterize the microporosity of silica/alumina-pillared montmorillonites. In both cases, the micropore size distributions, obtained using the H−K equation, revealed the existence of two sizes of micropores. They also found, in each case, that the microporosity was very dependent on the Al/clay ratio.

The microporosity of pillared clays was once thought to be determined by the d_{001} basal spacing (i.e., the interlayer spacing). However, from their studies of the adsorption characteristics of ZrO_2-pillared clays, Yang and Baksh[18] suggested that the pore sizes of certain pillared clays are limited not by the interlayer spacing, but, rather, by the interpillar spacing.

If the pore structure of pillared clays can be consistently and reliably controlled, it is conceivable, then, that pillared clays can be tailored for specific gas separations. Attempts to optimize the properties of pillared clays (mainly the overall surface area) have been typically focused on the effects of different pillaring agents and pillaring procedures. The choices of pillaring agents are numerous and many different pillared clays have been synthesized. However, the synthesis conditions, such as concentration of the metal ions, alkalinity or degree of hydrolysis (expressed as OH^-/M), temperature of preparation, time and temperature of aging, type of counterions, M/clay ratio, etc., can also have an affect on the physiochemical properties, including the microporosity, of the pillared clays.[1]

In this study, we have examined the effects of postsynthesis chemical modification on the microporous properties of Al_2O_3-pillared clays. These modifications were effected by incorporating different-sized charge-compensating alkali and alkaline earth cations into the pillared clay by standard ion-exchange techniques. The resulting materials were characterized with respect to their surface area, interlayer spacing, and micropore size distribution. We have chosen Al_2O_3-pillared clay for this study because of the small pore size and interlayer spacing of this material compared with other types of pillared clays (e.g., TiO_2-PILC, SiO_2-PILC).[1]

Experimental Section

Synthesis of the Pillared Clays. An experimental procedure similar to that of Fahey[19] was used in the synthesis of the pillared clays for this study. The resulting Al_2O_3-pillared clays were then modified by standard ion-exchange techniques.

A commercially available aqueous 50 wt % solution of hydroxy aluminum chloride, with an OH^-/Al molar ratio of approximately 2.5 and the approximate chemical formula of $Al_2(OH)_5Cl{\cdot}2H_2O$ (Chlorhydrol from Reheis Chemical Company) was used as the pillaring agent. The pillaring solution was prepared by adding 10 mL of the Chlorhydrol to 990 mL of deionized water. This solution was then aged, unstirred and at room temperature, for 14 days. One gram of purified bentonite clay (a Wyoming montmorillonite from Fisher with a typical unit cell formula of $Na_{0.8}[Al_{3.3}Mg_{0.5}Fe_{0.3}](Si_8)O_{20}(OH)_4$) was added to 45 mL of the aged Chlorhydrol solution. This slurry was then mixed for 1 h at 338 K in a heated water shaker bath. The solution was subsequently filtered and washed with deionized water until no precipitation was seen in the filter water upon treatment with a silver acetate solution. The filtrate was then placed in a conventional drying oven at 373 K for 1 h before being calcined in a furnace at 773 K for another hour. In the final calcination step, the intercalated oligomeric cation is decomposed into the metal oxide pillars, H_2O, and protons. The protons serve to balance the charge deficiency caused by the isomorphic substitution of Al^{3+} by Mg^{2+} in the octahedral layer of the montmorillonite and provide the pillared clay with its cation exchange capacity (CEC).

The resulting calcined pillared clays were thoroughly ground with a mortar and pestle before subsequent analysis or postsynthesis modification.

Ion Exchange. Ion exchange was accomplished by placing 1 g of the pillared clay into 30 mL of a concentrated salt solution of the desired exchange cation. The solution was prepared such that there were four exchange cations present (4X solution) for each milliequivalent of pillared clay. The Fisher purified bentonite has a CEC of 0.76 meq/g clay.[1] The solution was then heated until it reached a mild boil to accelerate the ion-exchange process. After allowing the solution to settle for an hour, the solution was decanted and another 4X solution of the same salt and concentration was added to the clay. This ion-exchange process was performed a total of three times before the resulting ion-exchanged pillared clays were filtered and washed with deionized water until no chloride remained. The resulting ion-exchanged material was then dried overnight at 373 K. The salts used for ion exchange were LiCl, NaCl, KCl, CsCl, and $MgCl_2$ (all from Strem Chemicals) and $CaCl_2$ (Aldrich).

Characterization. The surface areas and pore size distributions were determined from the nitrogen adsorption isotherms at 77 K. These isotherms were measured by a static volumetric method (Micromeritics ASAP 2010 adsorption analyzer). The samples were deaerated in vacuo at 623 K for a minimum of 4 h before analysis.

To obtain information about the micropore structure of the materials, it is necessary to collect adsorption data at very low relative pressures ($\sim 10^{-5}$ or lower). To do this, incremental doses of 5 mL/g of nitrogen were added to the approximately 0.2-g sample until a relative pressure of 0.04 was reached. Subsequent additions of nitrogen were made at volumes required to achieve a targeted set of relative pressures. A minimum equilibrium interval of 5 s with a tolerance of 5% of the target pressure (or 5 mmHg, whichever is smaller) was used for each measurement point.

X-ray diffraction data were obtained for a thin layer of the clays on a glass slide using a Rigaku rotating anode diffractometer with Cu Kα radiation.

(12) Everett, D. H.; Powl, J. C. *J. Chem. Soc., Faraday Trans.* **1976**, *72*, 619.
(13) Horvath, G.; Kawazoe, K. *J. Chem. Eng. Jpn.* **1983**, *16*, 470.
(14) Cheng, L. S.; Yang, R. T. *Chem Eng. Sci.* **1994**, *49*, 2599.
(15) Saito, A.; Foley, H. C. *AIChE J.* **1991**, *37*, 429.
(16) Gil, A.; Montes, M. *Langmuir* **1994**, *10*, 291.
(17) Gil, A.; Guiu, G.; Grange, P.; Montes, M. *J. Phys. Chem.* **1995**, *99*, 301.
(18) Yang, R. T.; Baksh, M. S. A. *AIChE J.* **1991**, *37*, 679.
(19) Fahey, D. R. U.S. Patent 4,845,066, 1989.

Theoretical Basis for Micropore Size Calculations. *Dubinin−Astakhov (D−A) Equation.* The development of the Dubinin−Radushkevich (D−R) equation was prompted by the failure to extend the theories governing adsorption on nonporous solids to that on real, porous solids, such as active carbons, synthetic zeolites, and dehydrated inorganic gels.[20] This lack of success led Dubinin and co-workers to focus their investigations on the problem of physical adsorption on porous materials and resulted in the Dubinin−Polanyi theory of micropore filling (also know as the theory of volume filling of micropores (TVFM)). This theory is based on the postulate that the mechanism for adsorption in micropores is that of pore filling rather than a layer-by-layer formation of a film on the walls of the pores. From this theory, Dubinin and Radushkevitch[21] arrived semiempirically at an expression that was later expanded by Dubinin and Astakhov[22] to give the Dubinin−Astakhov (D−A) equation

$$W = W_o \exp\left[-B\left(\frac{T}{\beta}\log\frac{P_o}{P}\right)^n\right] \quad (1)$$

where W is the volume adsorbed, W_o is the total micropore volume, and β is the affinity coefficient. The parameter B is related to the characteristic energy, E_o, by the following expression:

$$E_o = 0.001915\sqrt{(1/B)} \quad (2)$$

A theoretical derivation for the D−R and D−A equations has been given recently by Chen and Yang.[23,24] The D−A equation is simply a more generalized version of the D−R equation (where the parameter $n = 2$). Experimental evidence has revealed that $n \approx 2$ for activated carbonaceous sorbents[25] and approximately 4−6 for zeolites. The term "n" has been referred to as a "heterogeneity factor";[26] and, it has been suggested that it is related in some way to the heterogeneity (with respect to the pore distribution) of the surface.

The D−R and D−A equations have been effectively used to describe adsorption by microporous solids.[27] The D−R and D−A equations seem to be particularly useful in describing adsorption by microporous carbonaceous sorbents or activated carbons.[28]

Horvath−Kawazoe Equation. A theoretical framework was developed by Horvath and Kawazoe[13] for calculating the micropore size distribution from the steep-rise range of the isotherm (i.e., at very low relative pressures). The result, referred to as the Horvath−Kawazoe (H−K) equation, provides a simple relationship between the pore size and the relative pressure at which the pore is filled. Because of its simplicity, the H−K equation has been widely accepted. The H−K equation has been previously used to characterize the microporosity of carbonaceous,[13] and aluminosilicate[29] and aluminophosphate[30] zeolitic molecular sieves.

The H−K equation was originally derived for slit-shaped pores, and has since been extended to accommodate cylindrical[15] and spherical[14] pore geometries as well. Although the pore structures of pillared clays are quite complex, the slitlike pore geometry has been considered to be the most realistic of the available models.[15,16,31]

Improved H−K Equation. An implicit but important assumption made in the H−K development is linearity of the isotherm. Cheng and Yang[14] presented an improved H−K solution by considering the nonlinearity of the adsorption isotherm. Here the isotherm was represented by a Langmuir equation, which was representative of most isotherms.

The isotherms for adsorption in micropores under subcritical conditions (e.g., N_2 at 77 K) follow the typical type I behavior.[32] The Langmuir isotherm provides a good mathematical representation for type I isotherms. The assumption of linearity as made by Horvath and Kawazoe[13] was clearly inadequate; and although the region of steep rise is the only important area when determining the pore sizes, the use of Henry's law would have missed the isotherm data in the concave portion of the steep rise.[14] Consequently, if the Henry's law region is replaced by the Langmuir-type equation of state, the result is the improved H−K equation (or as the H−K equation with the Cheng−Yang correction). The improved H−K equation for slit-shaped pore geometries is as follows

$$RT\ln\left(\frac{P}{P_o}\right) + \left[RT - \frac{RT}{\theta}\ln\frac{1}{1-\theta}\right] = N_{AV}\frac{N_a A_a + N_A A_A}{\sigma^4(L-2d_o)}\left[\frac{\sigma^4}{3(L-d_o)^3} - \frac{\sigma^{10}}{9(L-d_o)^9} - \frac{\sigma^4}{3d_o^3} + \frac{\sigma^{10}}{9d_o^9}\right] \quad (3)$$

From the amount adsorbed at P, eq 3 yields the corresponding slit-pore width, L; thus, the pore volume at pore size L is known. Equation 3 reduces to the original H−K equation with the removal of the second term on the left side.

Results and Discussion

As mentioned earlier, our goal in this study was to examine the effects of postsynthesis ion exchange on the microporous properties of Al_2O_3-pillared clays. These modifications were effected by incorporating differently-sized charge-compensating cations from the alkaline and alkaline earth series into the pillared clay by standard ion-exchange techniques. The resulting materials were characterized with respect to their surface area, interlayer spacing, and micropore size distribution.

The samples and analytical results are identified by the following convention: the sample Li^+−PILC represents Al_2O_3-pillared clay which has undergone postsynthesis ion exchange with the Li^+ cation (in a solution of LiCl as described earlier). The unaltered Al_2O_3-pillared clay may, at times, be referred to as H^+−PILC, because prior to any postsynthesis ion exchange, the proton is the charge-compensating cation in the calcined pillared clay.

X-ray Diffraction. XRD patterns of the (001) reflectance for the unpillared purified bentonite, the unaltered original Al_2O_3-pillared clay, and the Li^+, Na^+, and K^+ ion-exchanged clays are shown in Figure 1. Basal spacings (d_{001}) corresponding to the maximum in these patterns are given in Table 1. The 2θ angle of the (001) basal reflection was 7.1° for the unpillared purified bentonite and 5.1° for the unaltered Al_2O_3−PILC, which corresponds to d_{001} basal spacings of 1.21 nm for the unpillared clay and 1.69 nm for the Al_2O_3−PILC. The d_{001} spacing for the Li^+, Na^+, and K^+ ion-

(20) Hutson, N. D.; Yang, R. T. *Adsorption* **1997**, *3*, 189.
(21) Dubinin, M. M.; Radushkevitch, L. V. *Proc. Acad. Sci. USSR* **1947**, *55*, 331.
(22) Dubinin, M. M.; Astakhov, V. A., *Izv. Akad. Nauk SSR, Ser. Khim.* 1971.
(23) Chen, S. G.; Yang, R. T. *Langmuir* **1994**, *10*, 4244.
(24) Chen, S. G.; Yang, R. T. *J. Coll. Interface Sci.* **1996**, *177*, 298.
(25) Dubinin, M. M. *Progress in Surface and Membrane Science*, Cadenhead, D. A., Eds.; Academic: New York, 1975.
(26) Rudzinski, W.; Everett, D. H. *Adsorption of Gases on Heterogeneous Surfaces*; Academic: London, 1990.
(27) Huber, H.; Stoeckli, H. F.; Houriet, J. Ph. *J. Colloid Interface Sci.* **1978**, *67*, 195.
(28) Dubinin, M. M.; Stoeckli, H. F. *J. Colloid Interface Sci.* **1980**, *75*, 34.
(29) Venero, A. F.; Chiou, J. N. *MRS Symp. Proc.* **1988**, *111*, 235.
(30) Davis, M. E.; Montes, C.; Hathaway, P. E.; Arhancet, J. P.; Hasha, D. L.; Garces, J. E. *J. Am. Chem. Soc.* **1989**, *111*, 3919.
(31) Baksh, M. S. A.; Yang, R. T. *AIChE J.* **1992**, *38*, 1357.
(32) Gregg, S. J.; Sing, K. S. W. *Adsorption, Surface Area and Porosity*, 2nd ed.; Academic: London, 1982.

Table 1. Basal Spacings (d_{001}) and Mesopore Characteristics for the Unmodified Al_2O_3−Pillared Clay and the Ion-exchanged Pillared Clays

clay	d_{001} (nm)	cumulative surface area of pores[a] (m^2/g)	mesopore volume[a] (mL/g)	peak mesopore width[a] (nm)	incremental pore area at peak[a] (m^2/g)	Langmuir SA (m^2/g)	BET SA (m^2/g)
unpillared	1.21						
Al_2O_3−PILC	1.69	65.5	0.11	2.33	8.6	431	324
Li^+−PILC	1.69	57.9	0.10	2.32	7.6	385	290
Na^+−PILC	1.69	56.2	0.10	2.32	7.6	393	296
K^+−PILC	1.67	58.7	0.10	2.33	7.6	416	313
Cs^+−PILC		51.9	0.10	2.32	6.6	406	306
Mg^{2+}−PILC		54.2	0.10	2.32	7.0	395	297
Ca^{2+}−PILC		57.4	0.10	2.32	7.7	419	314

[a] Determined by the BJH adsorption method (for pores 1.7−300 nm).

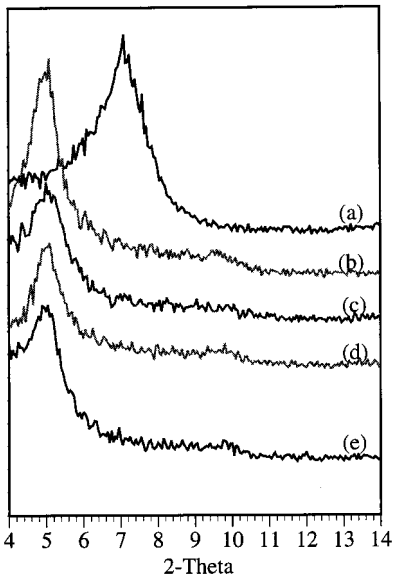

Figure 1. X-ray diffraction patterns for (a) unpillared purified bentonite, (b) unmodified Al_2O_3−PILC, (c) Li^+−PILC, (d) Na^+−PILC, and (e) K^+−PILC.

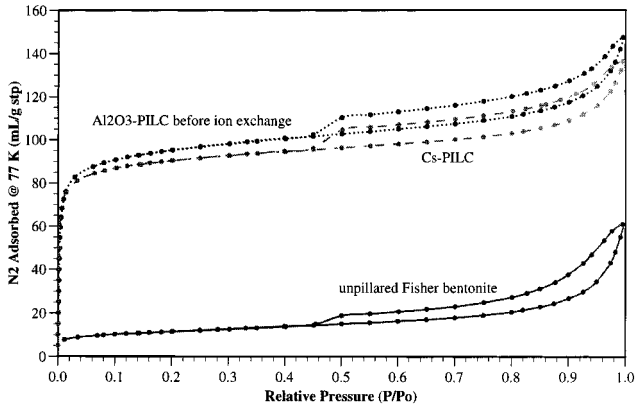

Figure 2. Nitrogen isotherms at 77 K for unmodified Al_2O_3−PILC, Cs^+−PILC, and unpillared purified bentonite.

exchanged PILCs were also approximately 1.69 nm, indicating no change in the interlayer spacing upon alteration of the pillared clay by postsynthesis ion exchange.

Adsorption Isotherms. The adsorption and desorption isotherms for the unpillared clays, the unaltered pillared clay, and the Cs^+ ion-exchanged pillared clay are shown in Figure 2. All of these isotherms correspond to the type I isotherm according to the Brunauer, Deming, Deming, and Teller (BDDT) classification.[33] The general aspect of the isotherms shown (and for those of the other ion-exchanged clays) has not changed from that of the original pillared or unpillared clay. Figure 3 shows the low-pressure region for the Cs^+ ion-exchanged pillared bentonite and for the unaltered pillared bentonite.

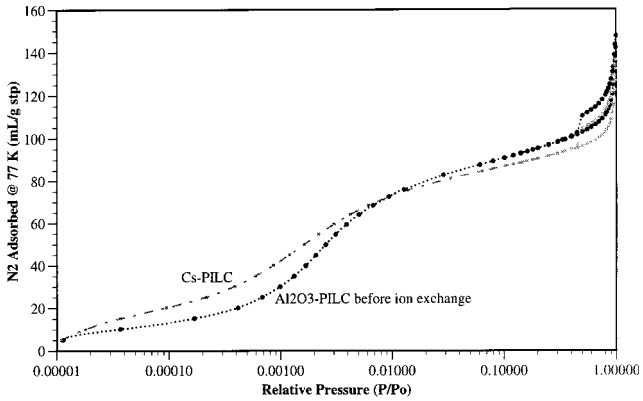

Figure 3. Low-pressure isotherms for unmodified Al_2O_3−PILC and Cs^+−PILC.

Mesoporosity and Surface Area. The hysteresis loop present in all of the displayed isotherms indicates the presence of mesoporosity. The mesoporosity of each of the samples was characterized using the Barrett−Joyner−Halenda (BJH) method.[34] A summary of the mesoporosity of each of the pillared clays, as determined by the BJH analysis, is given in Table 1. One can see that the mesopore structure of the clays does not seem to be significantly affected by the ion-exchange process. Each of the pillared clays (including the unaltered Al_2O_3−PILC) has a peak mesopore width at approximately 2.32 nm. There is a slight decrease in mesopore volume (for pores between 1.7 and 300 nm) with the ion exchange. The mesopore volume for the unaltered Al_2O_3−PILC was 0.111 mL/g, whereas that of the Cs^+ ion-exchanged material had decreased to 0.095 mL/g. Likewise, there is a corresponding decrease in the cumulative mesopore surface area from 65.50 m^2/g for the unaltered pillared clay to 51.92 m^2/g for the Cs^+ ion-exchanged clay.

The surface area of the ion-exchanged pillared clays was determined using both the BET equation and the Langmuir equation for isotherm data between $0.05 < P/P_o < 0.2$. Although the BET surface area is the more

(33) Sing, K. S. W.; Everett, D. H.; Haul, R. A. W.; Moscou, L.; Pierotti, R. A.; Rouguerol, J.; Siemieniewska, T. *Pure Appl. Chem.* **1985**, *57*, 603.

(34) Barrett, G. P.; Joyner, L. G.; Halenda, R. H. *J. Am. Chem. Soc.* **1951**, *73*, 373.

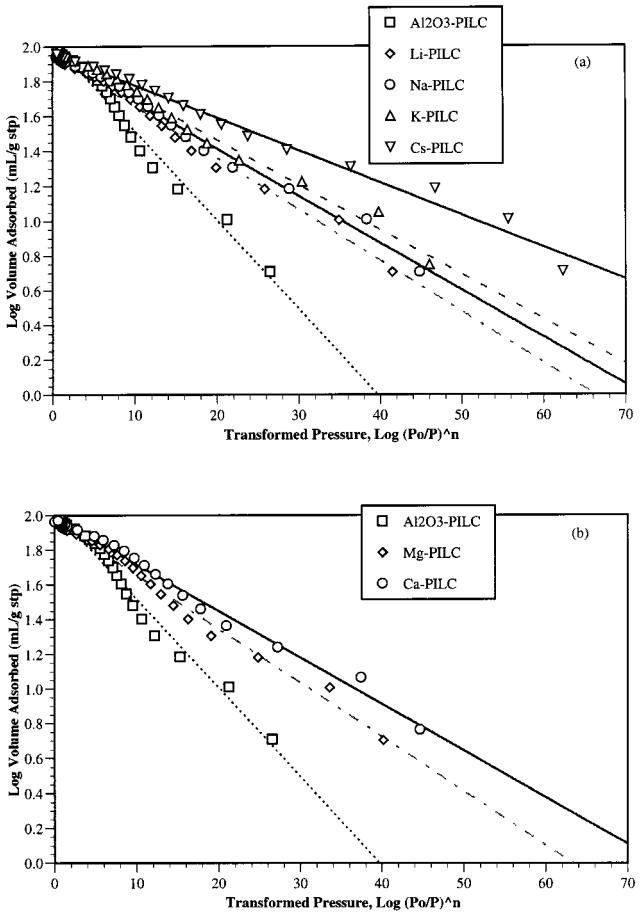

Figure 4. Dubinin−Astakhov (D−A)-transformed isotherms for the unmodified Al_2O_3−PILC and (a) monovalent cation-exchanged clays, and (b) divalent cation-exchanged clays.

commonly reported, it has been suggested that the Langmuir equation for monolayers is more appropriate for microporous solids than the BET equation for multilayers.[4,16,35] The results for both are given in Table 1. In each case, the surface areas (Langmuir and BET) of the ion-exchanged pillared clays are lower than that of the unaltered Al_2O_3−PILC.

Dubinin−Astakhov (D−A)-Transformed Isotherms. Dubinin-Astakhov (D−A)-transformed isotherms are plots of $\log(W)$ versus $\log(P_o/P)^n$ (which is from a linearization of the D−A equation (eq 2)) and are analogous to the more commonly presented D−R plot. These D−A-transformed isotherms were plotted for each of the ion-exchanged samples and are shown in Figure 4. On the basis of the principles of micropore filling, a D−R (and thus a D−A) plot should be linear (assuming a Gaussian micropore size distribution), and the intercept should equal $\log(W_o)$, where W_o is the micropore volume (assuming the pores are filled with liquid adsorbate).[36−38] All of these D−A plots show several deviations from linearity, suggesting the presence of multiple types of micropores (i.e., D−A plots with two different linear regions possess two kinds of micropores). The micropore volumes obtained from the D−A equation analysis for each of the pillared clays are given in Table 2. Micropore volumes obtained from the H−K equation are also given in Table 2 and show good agreement with the D−A micropore volumes.

Table 2. D−A Equation Heterogeneity Factor and the Characteristic Energy for the Unmodified Al_2O_3−Pillared Clay and the Ion-Exchanged Pillared Clays

clay	heterogeneity factor, *n*	characteristic energy, kJ/mol	micropore vol[a] (mL/g)	micropore vol[b] (mL/g)
unpillared				
Al_2O_3−PILC	2.05	4.22	0.163	0.149
Li^+−PILC	2.33	4.70	0.138	0.132
Na^+−PILC	2.37	4.74	0.140	0.135
K^+−PILC	2.39	4.84	0.148	0.143
Cs^+−PILC	2.58	5.03	0.142	0.142
Mg^{2+}−PILC	2.32	4.62	0.143	0.138
Ca^{2+}−PILC	2.39	4.75	0.149	0.143

[a] Determined from the D−A equation. [b] Determined from the H−K equation (slit pore model using the Cheng−Yang correction).

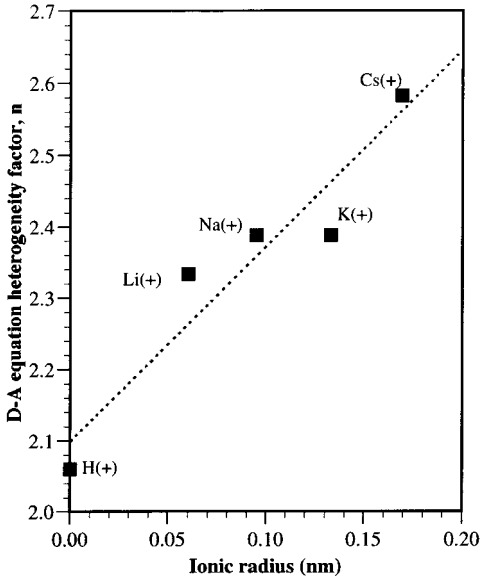

Figure 5. Dubinin−Astakov (D−A) equation heterogeneity factor, *n*, versus ionic radius of the charge-compensating cation.

The optimized value of the heterogeneity factor, *n* for each of these clays, along with the overall characteristic energy, *E*, are given in Table 2. Each of the ion-exchanged pillared clays has a heterogeneity factor of $2 < n < 3$, which is very similar to the value of 2 expected for activated carbons.[25] In general, the heterogeneity factor and the characteristic energy tend to increase with the ionic radius of the charge compensating cation used in the ion-exchange process. This result indicates a trend toward greater structural and energetic heterogeneity with incorporation of larger sized cations. This heterogeneity is shown in Figure 5 and Figure 6.

Micropore Size Distribution. The micropore size distribution for the pillared clays was calculated with the improved Horvath−Kawazoe (H−K) equation (i.e., with the Cheng−Yang correction) for slit-pore geometry. The H−K equation parameters used in this evaluation (to calculate the interaction parameter) are shown in Table 3. The micropore size distributions for the ion-exchanged pillared clays are shown in Figure 7 and, in

(35) Occelli, M. L.; Finseth, D. H. *J. Catal.* **1986**, *99*, 316.
(36) Rodriguez-Reinoso, F.; Garrido, J.; Martin-Martinez, J. M. *Carbon* **1989**, *27*, 23.
(37) Kakei, K.; Ozeki, S.; Suzuki, T.; Kaneko, K. *J. Chem. Soc., Faraday Trans.* **1990**, *86 (2)*, 371.
(38) Atkinson, D.; McLeod, A. I.; Sing, K. S. W. *J. Chim. Phys.* **1984**, *81*, 791.

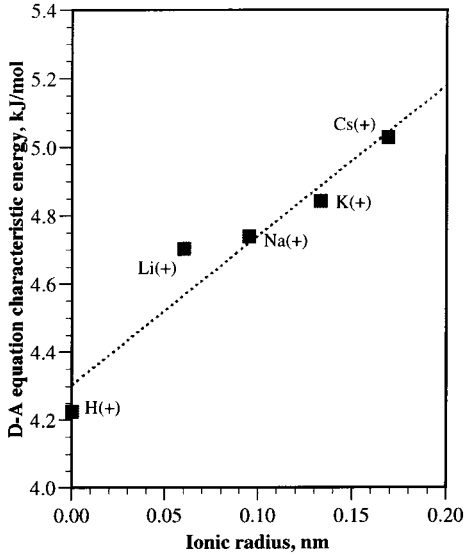

Figure 6. Dubinin−Astakov (D−A) equation characteristic energy (kJ/mol) versus ionic radius of the charge-compensating cation.

Table 3. Horvath−Kawazoe Equation Parameters[a]

parameter	adsorbent (aluminosilicate)	adsorptive (nitrogen @ 77 K)
diameter, nm	0.2760	0.3000
diameter at zero energy, nm	0.2369	0.2574
polarizability, cm^3	2.5×10^{-24}	1.76×10^{-24}
magnetic susceptibility, cm^3	1.3×10^{-29}	3.6×10^{-29}
density, molec/cm^2	1.31×10^{15}	6.71×10^{14}

[a] From ref 14.

each case, are plotted along with that of the unaltered Al_2O_3-pillared clay for comparison. An overlay of each of these pore size distributions for both the monovalent and divalent ion-exchanged clays is given in Figure 8. Each of the ion-exchanged pillared clays showed a bimodal micropore size distribution that is broader and less symmetrical than that of the unaltered PILC. The bimodal micropore distribution was predicted from the D−A-transformed isotherms and is consistent with previously reported distributions for similar clays.[16] The materials all have micropores having distributions with maxima at about 0.38 and 0.53 nm. One can see that there is an increase in the micropore volume at the lower pore size with increasing ionic radius. The micropore volumes were integrated for the two types of micropores (i.e., <0.45 nm and >0.45 nm) and the results are given in Table 4. The micropore volume for those pores in the lower range increased with an increase in the ionic radius of the charge compensating cation as shown in Figure 9.

The effect on the micropore volume for those pores in the larger range is not as predictable. All of the ion-exchanged PILCs had a micropore volume that was less than that of the unaltered Al_2O_3−PILC (the H^+−PILC). The Li^+, Na^+, and Cs^+ ion-exchanged pillared clays had comparable micropore volumes. However, the K^+ ion-exchanged pillared clay, unexpectedly had a larger micropore volume than the other ion-exchanged clays. These results, along with the corresponding total micropore volumes, are shown in Figure 9. Figure 10 shows a plot of the percentage of micropores of each type (i.e., those <0.45 nm and those >0.45 nm). This plot

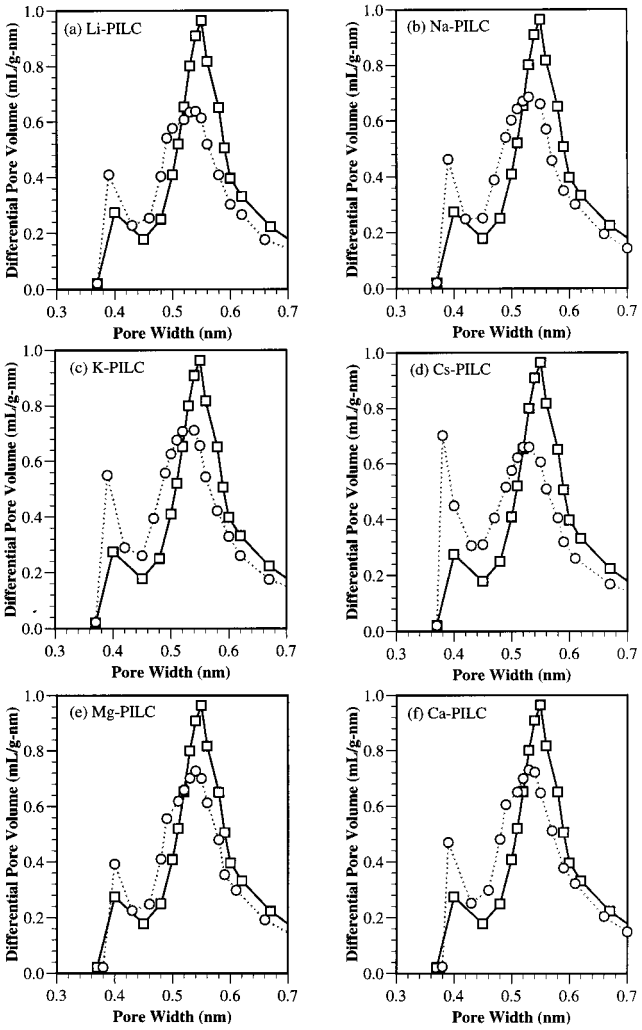

Figure 7. Micropore size distribution for the ion-exchanged pillared clays (dashed lines) and the unmodified Al_2O_3−PILC (solid lines): (a) Li^+−PILC, (b) Na^+−PILC, (c) K^+−PILC, (d) Cs^+−PILC, (e) Mg^{2+}−PILC, and (f) Ca^{2+}−PILC.

Table 4. Micropore Volumes for the Unmodified Al_2O_3−Pillared Clay and the Ion-Exchanged Pillared Clays

clay	pore volume (mL/g) <0.45 nm	pore volume (mL/g) >0.46 nm
Al_2O_3−PILC	0.024 (15.8%)	0.126 (84.2%)
Li^+−PILC	0.029 (21.7%)	0.103 (78.3%)
Na^+−PILC	0.031 (23.1%)	0.104 (76.9%)
K^+−PILC	0.034 (24.0%)	0.109 (76.0%)
Cs^+−PILC	0.039 (27.4%)	0.103 (72.6%)
Mg^{2+}−PILC	0.031 (22.5%)	0.107 (77.5%)
Ca^{2+}−PILC	0.036 (25.0%)	0.107 (75.0%)

shows a clear trend of decreasing pore volume (as a percentage of the total) for the pores >0.45 nm with incorporation of increasing cation radius. There is a corresponding trend toward larger pore volume for those pores <0.45 nm with increasing cation radius. The unaltered H^+−PILC had a pore volume for pores of <0.45 nm, which was 16% of the total micropore volume. However, with the incorporation of the Cs^+ ion, the largest of the alkali cations used, the micropores in the lower range had a volume that was more than 27% of the total.

It is obvious that the microporosity of the pillared clay has been affected by the incorporporation of alkaline and

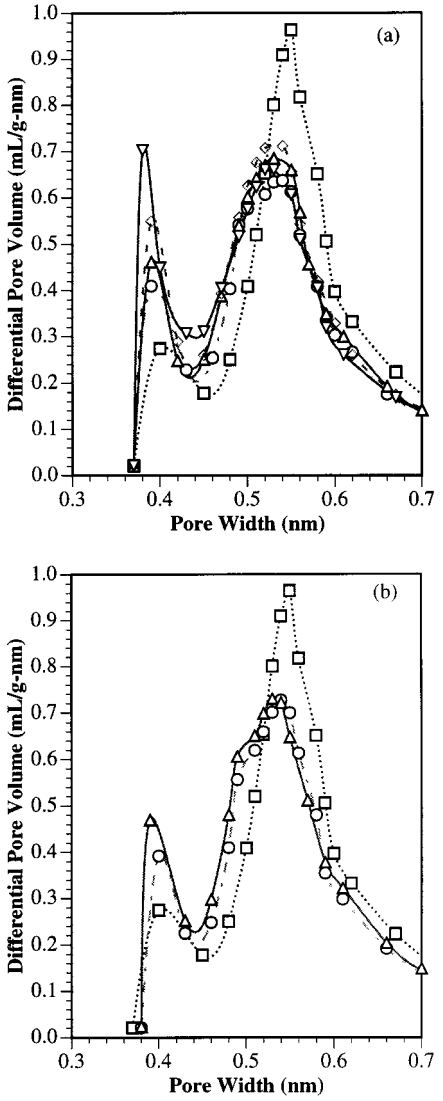

Figure 8. Overlays of the micropore size distributions of the unmodified Al_2O_3−PILC and (a) monovalent cation-exchanged clays, and (b) divalent cation-exchanged clays.

alkaline earth metals by ion exchange. To understand this effect, it is important to understand where the charge-compensating cations are located in the pillared clay. One influence on the interlayer cation location is the type of clay used. The location of the charge deficit for dioctahedral substituted clays (e.g., montmorillonites) is in the octahedral layer.[10] The actual position of the exchanged alkali and alkaline earth cations depends on the size of the cation and the energy that it possesses during the calcination step.[39] Tettenhorst[40] studied the migration of various cations in montmorillonites and found that the extent of migration into the clay is affected little by the charge or polarizing power of the cation. The author also suggested that most cations do not migrate to octahedral sites but, instead, to hexagonal Si−O cavities within the interlayer space. A schematic of this suggestion is shown in Figure 11. The author also points out that cations in this location are more tightly held because they are closer to the locus of the charge deficiency, and that the basal oxygen

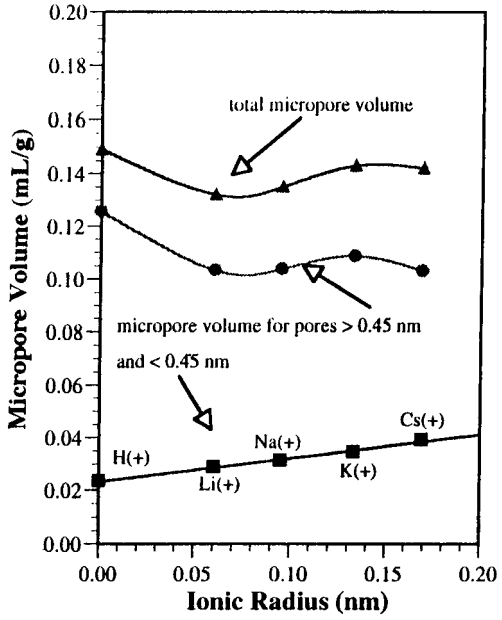

Figure 9. Micropore volume (total and for pores >0.45 nm and <0.45 nm) versus ionic radius of the charge-compensating cation.

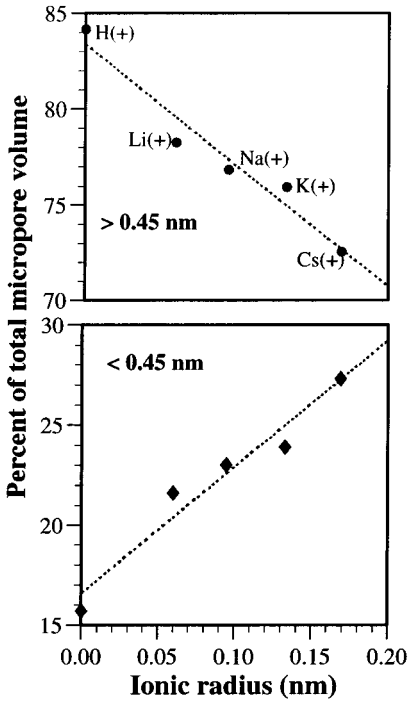

Figure 10. Percentages of total micropore volumes for those >0.45 nm (top) and those <0.45 nm (bottom).

layers of adjacent units are closer because the cations have migrated from the interlayer positions, which would tend to seal off the avenues of accessibity of the cation.

Calvet and Prost[41] used infrared (IR) spectroscopy to study the migration of cations in heated ion-exchanged montmorillonites. The results indicated that, upon calcination, a small fraction of lithium ions move within the clay structure toward the octahedral sites that lie near the isomorphic substitutions. Some of the remain-

(39) Grim, R. E. *Clay Mineralogy*, McGraw-Hill: New York, 1968.
(40) Tettenhorst, R. *Am. Mineral.* **1962**, *47*, 769.
(41) Calvet, R.; Prost, R. *Clays Clay Miner.* **1971**, *19*, 175.

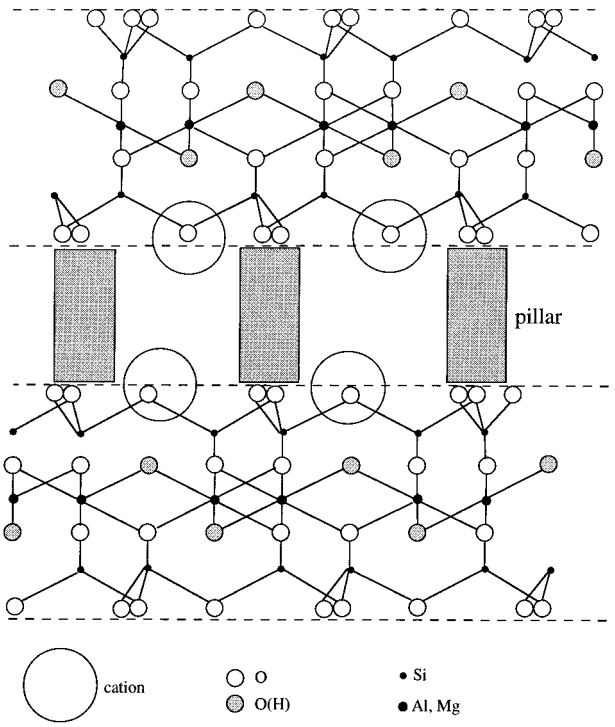

Figure 11. Schematic of pillared clay structure with cation location.

ing lithium ions are present at accessible interlayer sites, with others being trapped in hexagonal cavities in the interlayer space. The authors also reported that although some Mg^{2+} ions also migrate to empty octahedral sites, Ca^{2+} and larger cations probably do not; rather, they may be localized in the bottom of hexagonal cavities in the interlayer space. The authors also suggested that structural modifications take place with the cation migration and create local trioctahedral configurations.

For the unaltered Al_2O_3−PILC (the H^+−PILC), the charge-compensating protons are most likely located in open sites within the octahedral layer, which leaves a completely open clay surface with no hindrances within the micropores. This material should, and does, have the largest surface area and the highest total micropore volume. The addition of the Li^+ ion creates a material in which some of the Li^+ ions are located within the clay structure at the octahedral layer, others are located in accessible locations within the interlayer space, and others are located in hexagonal cavities in the interlayer space. The structural modifications that take place with the cation migration to the hexagonal cavities would account for the decrease in the surface area from the H^+−PILC to the Li^+−PILC (given earlier in Table 1). Based on the findings of Tettenhorst[40] and Calvet and Prost,[41] as described earlier, it is unlikely that any of the alkaline metal cations larger than Li^+ will be incorporated into the octahedral layer of the PILC with heating. It must be assumed, then, that these cations are located entirely in accessible locations within the interlayer space and in hexagonal cavities in the interlayer space. A greater number of accessible cations in the interlayer space should tend to increase the surface area of the Na^+, K^+, and Cs^+ ion-exchanged PILCs over that of the Li^+−PILC. This expected result corresponds to the actual data (given earlier in Table 1).

The suggested structural modifications that take place with the migration of cations to interlayer hexagonal cavities can also be used to explain some of the effects of ion-exchange on the microporous properties of the PILCs. The ion exchanged pillared clays all displayed a bimodal micropore size distribution, which is consistent with the result of the unaltered Al_2O_3−PILC. The pore size distributions for the ion-exhanged PILCs are broader and less symmetrical than that of the unaltered PILC. The surprising result, however, is that there is only a slight shift in the pore size distribution from the unaltered PILC to the ion-exchanged PILCs. The ion-exchanged materials all have micropore distributions with maxima at about 0.38 and 0.53 nm. This result is surprising because alkali and alkaline earth metal cations are used to control the size of pore openings in A-type zeolites, which is not the case with the pillared clays. There is only a change in the pore volume, and a corresponding shift in the percentage of total micropore volume from the larger pores (> 0.45 nm) to the smaller pores (<0.45 nm). This shift is most likely due to pore blockage in the larger pores, resulting in a greater number of pores in the 0−0.45-nm range, and thus a greater micropore volume in that range.

The interlayer spacing for these pillared clays is found by subtracting the thickness of the bentonite clay layer (0.96 nm) from the (001) basal spacing of pillared clays (1.69 nm), giving a interlayer spacing of approximately 0.73 nm. Given that the micropores have a distribution centered at about 0.38 and 0.53 nm, it is obvious that the micropore size is limited by the interpillar distance rather than by the interlayer distance.

Although the Li^+, Na^+, and K^+ cations will be positioned in the Si−O hexagonal holes in the interlayer space, the Cs^+ ion will not fit into those holes. In fact, because the Cs^+ ionic diameter is approximately 0.34 nm, the micropores will likely sterically hinder ready ion exchange of the Cs^+ ion. Also, it is highly unlikely that there is any back-to-back positioning of the Cs^+ ions within the interlayer space. These limitations in the ion exchange of Cs^+ help to explain some of the results seen with this particular clay (e.g., lower total surface area than the K^+−PILC).

The accuracy of the calculation of the micropore size distribution by the H−K equation is very dependent on the accuracy of the calculation of the H−K interaction parameter and on the actual accessibility of the microporous pillared clays. However, the result of a bimodal pore size distribution and the corresponding micropore volumes are consistent with the results of the evaluation using the D−R equation. Density functional theory (DFT) methods[42] were also used to characterize the microporosity of the pillared clays, but the results were inconsistent with those of the H−K equation and with the XRD data. The interlayer spacing, as determined by subtracting the clay layer thickness (0.96 nm) from the (001) basal spacing of the pillared clays (1.69 nm), was approximately 0.73 nm. However, when DFT methods (original DFT model, slit-pore geometry[43]) were

(42) Balbuena, P. B.; Gubbins, K. E. *Fluid Phase Equilibria* **1992**, *76*, 21.
(43) DFT Plus Models Library User's Guide V1.00, Micromeritics Instrument Corp., 1996.

used to determine the pore-size distribution, a single peak at 1.179 nm was given for all the samples and no microporosity less than 1.0 nm was indicated. This peak, at 1.179 nm, is much larger than the interlayer spacing given by XRD analysis. Because of these inconsistencies, the DFT data are not given.

Acknowledgment. This work was supported by the National Science Foundation under Grant CTS-9520328.

Nomenclature

B = parameter in D−R, D−A equations, related to E_o
d_0 = arithmetic mean of diameters of adsorbate and adsorbent atoms
E = characteristic energy of adsorption; energy
E_o = characteristic energy of adsorption for standard vapor
n = parameter in D−A equation, heterogeneity factor
L = distance between nuclei of the opposite pore walls
N = density per unit area
N_{AV} = Avogadro's number
P = pressure
P_o = saturated vapor pressure
R = gas constant
T = temperature
W = volume of micropores filled at relative pressure P/P_o
W_o = total volume of micropore system
z = distance of adsorbate molecule from a surface atom in pore

Greek symbols

β = similarity coefficient
θ = degree of void filling
ϵ = potential energy of interaction
σ = distance from an atom in the surface layer at zero interaction energy

CM980454J